ChemComm

COMMUNICATION

View Article Online
View Journal



Cite this: DOI: 10.1039/d6cc00572a

Received 28th January 2026,
Accepted 19th April 2026

DOI: 10.1039/d6cc00572a

rsc.li/chemcomm

# Discrimination of aliphatic and aromatic hydrocarbons *via* modulated folding and fluorescence of an NDI-tetramer

Dhanyashree Das, Dhrubajyoti Talukdar and Bappaditya Gole *

**We report the synthesis of an electroactive, conformationally flexible NDI tetramer and its solvent-dependent folding. While both aliphatic and aromatic hydrocarbons facilitate its folding, the former enhances excimer emission, whereas the latter quenches emission by favouring the charge transfer process. This contrasting emission behaviour enables a rare differentiation between aliphatic and aromatic hydrocarbons.**

Nature employs biomacromolecular folding as a fundamental strategy to manifest sophisticated functions essential for the survival of living systems. Inspired by this principle, synthetic foldamers have emerged as promising artificial analogues that mimic the structure and functions of biopolymers.[1–3] While helical foldamers have been extensively explored, sheet-like foldamers, reminiscent of β-sheets in proteins, remain comparatively limited, particularly when constructed from π-conjugated dyes.[4–11] Such structural architectures provide unique opportunities to generate co-facial chromophore stacks, enabling excitonic coupling and photoinduced charge separation.[12–16] Consequently, they have gained considerable attention as a new class of functional materials in recent years owing to their discrete molecular structures and tunable photophysical properties. Recent reports demonstrated their prospects in light harvesting, charge separation, transport, and catalysis.[17–20] In contrast to the conventional dye assemblies, which rely on weak noncovalent interactions and often suffer from uncontrolled aggregation and structural ambiguity, these covalently linked oligomeric systems offer predictable structural features with discrete dye stacks and exciting photophysical responses. However, achieving controlled folding in such systems remains a major obstacle. While rigid oligomers typically adopt predictable folded conformations, flexible systems are inherently dynamic, populating both folded and unfolded states in solution.[21,22] Nevertheless, enabling folding of such systems offers a photophysical property that is absent in the unfolded state, thereby acting as a responsive system. For example, solvent-dependent phenomena observed in merocyanine oligomers, where solvent polarity governs stepwise folding and leads to distinct photophysical properties, highlight it as a simple and effective strategy for tuning folding and function.[23,24] Among the limited dye-appended oligomers explored so far, naphthalene diimide (NDI) is especially attractive due to its versatile optical and electrochemical properties.[25,26] Recently, NDI oligomers have been reported to show multielectron redox behavior and catalytic activity.[19,20] The rigid backbones present in those cases were critical in obtaining a long-range order in the solution. In contrast, flexible NDI oligomers capable of adaptive folding behaviour in solution remain scarce and, so far, limited to dimeric systems.[27]

Herein, we report the synthesis of a covalently linked, discrete, and conformationally flexible NDI tetramer, **1**. In chlorinated solvents, where NDI derivatives are known to be efficiently solvated, **1** adopts a partially folded state and exhibits pronounced excimer emission. The addition of nonpolar solvents, aliphatic and aromatic, further reinforces folding, leading to solvent-dependent modulation of its emission property. Even though both classes of solvents promote folding, they induce contrasting emission responses. While aliphatic solvents enhance excimer emission, the aromatic counterpart quenches it through charge-transfer (CT) processes between the electron-deficient oligomer and electron-rich guests and provides a weak CT emission. This dual response enables differentiation between aliphatic and aromatic hydrocarbons, a rarely explored and challenging task, and underscores the potential of flexible NDI foldamers as responsive materials.

The NDI tetramer **1** (Fig. 1a) was synthesized *via* a convergent multistep strategy, as outlined in Schemes S1–S3. The pyridine linkers connecting the NDI units serve as turn units that promote organized stacking of the chromophores into a folded, sheet-like arrangement. Alkyl spacers between the pyridine and NDI units impart conformational flexibility. Detailed experimental procedures can be found in the SI.

Oligomer **1** was characterized using nuclear magnetic resonance (NMR), mass, UV-Vis and fluorescence spectroscopy. The $^1$H-NMR spectrum recorded in $CDCl_3$ at 298 K displays well-resolved, sharp signals, consistent with a discrete molecular structure (Fig. 1b).

*Biomimetic Supramolecular Chemistry Laboratory, Department of Chemistry, School of Natural Sciences, Shiv Nadar Institution of Eminence Deemed to be University, Greater Noida, Uttar Pradesh 201314, India. E-mail: bappaditya.gole@snu.edu.in*

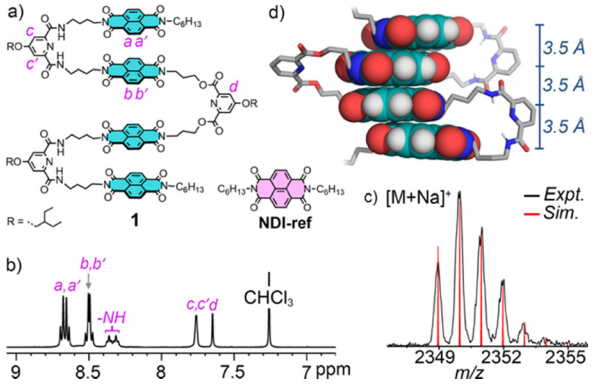


Fig. 1 (a) Chemical structure of **1** and reference **NDI-ref**. (b) Selected region 400 MHz $^1$H-NMR spectrum of **1** (5 mM) in $CDCl_3$ at 298 K. (c) MALDI-TOF mass spectra of **1** with simulated isotopic mass distribution. (d) The energy-minimized model of **1** with distances between NDI units. Side chains are omitted for clarity.

Two sets of NDI resonances are observed at 8.67 and 8.50 ppm (four protons each), assigned to the outer and inner NDI units, respectively, reflecting the symmetry that divides the oligomer into two halves. Similarly, two distinct pyridine proton signals appear at 7.75 and 7.65 ppm in a 2 : 1 ratio. The sharp signal at 7.65 ppm corresponds to the inner pyridine proton, while the relatively broader signal at 7.75 ppm is attributed to the two protons of the outer pyridine, which experience slightly different but closely related chemical environments. The amide protons resonate at 8.32 and 8.35 ppm, as confirmed by $^1$H-$^{15}$N HSQC experiments (Fig. S2). The weak coupling of the NDI proton signals indicates a uniform chemical environment with minimal perturbation from terminal functionalities. Notably, the upfield shift of the inner NDI compared to the outer NDI suggests an ordered structure of the oligomer, where the inner NDIs face a significant ring current. MALDI-TOF mass spectrometry shows an isotopic distribution in excellent agreement with the simulated pattern, confirming the molecular identity of **1** (Fig. 1c and Fig. S3). Together, these analyses establish the formation and purity of the compound.

To examine the temperature dependency of **1**, variable-temperature $^1$H-NMR spectra were recorded in $CDCl_3$ over the range of 298–323 K (Fig. S4). The NDI and pyridine proton resonances exhibit no significant change; however, the amide proton signals became sharper and significantly upfield-shifted, due to destabilization of H-bonding with pyridine nitrogen. Concentration-dependent $^1$H-NMR measurements between 0.5 and 5 mM showed no significant spectral changes (Fig. S5), excluding intermolecular aggregation. Attempts to grow single crystals were unsuccessful, likely due to the conformational flexibility of the oligomer. Therefore, to gain structural insight, geometry optimization was performed using the Universal Force Field (UFF) in the Forcite module of Materials Studio. The optimized structure reveals a folded conformation in which the NDI units stack with interlayer separations of nearly 3.5 Å (Fig. 1d). The calculated solvodynamic diameter obtained from DOSY NMR in $CDCl_3$ is ~27 Å (Fig. S6), which is much higher than the theoretical molecular length of ~11 Å. It indicates the dynamic nature between folded and unfolded states of **1** in solution.

The absorption spectrum of **1** in DCM displays characteristic features of the $S_0$–$S_1$ transition with maxima at 381 nm ($A_{0-0}$) and vibronic progression at 361 nm ($A_{0-1}$) and 340 nm ($A_{0-2}$), closely resembling those of the reference, **NDI-ref** (Fig. 2a). However, lower molar absorptivity of **1** ($1.0 \times 10^5$ $M^{-1}$ $cm^{-1}$) than four times that of **NDI-ref** ($2.95 \times 10^4$ $M^{-1}$ $cm^{-1}$), indicates electronic interaction between NDIs. The emission property of **1** differs distinctively from **NDI-ref**, which has only weak monomeric fluorescence. It exhibits an additional broad excimer emission centered at 493 nm upon excitation at 360 nm (Fig. 2a). The emergence of strong excimer emission from **1** even at a low concentration (0.5 μM) highlights inter-NDI interactions within the oligomer (Fig. S7). Only a limited NDI-derivatives show excimer emission, but at much higher concentrations.[28] Importantly, no excimer emission can be observed for **NDI-ref** even at a 1 mM concentration (Fig. S8). The dimeric analog **10** shows excimer emission, but it is much weaker than **1** (Fig. S10). The concentration-dependent enhanced excimer emission (Fig. S7) observed in **1** may indicate a prevailing folded state. Noted that even though the absorbance of $A_{0-0}$ and $A_{0-1}$ bands varies linearly within the concentration range in UV-Vis studies, the $A_{0-0}/A_{0-1}$ ratio (1.16) at 3 μM decreased to 1.07 at 54 μM (Fig. S9). It provides evidence of folding and excludes intermolecular association. The fluorescence lifetime was measured to be 19.9 ns, consistent with excimer emission (Fig. S11). Overall, these studies indicate that **1** is dominantly populated in a partially folded state in $CHCl_3$, if not completely folded.

The redox behaviour of **1** was investigated by cyclic voltammetry (CV) in DCM using $Bu_4NPF_6$ as the supporting electrolyte. The CV shows multiple reversible reduction processes at $E_{1/2}$ = −0.72, −0.86, −0.95, and −1.27 V *versus* $Fc/Fc^+$ (Fig. 2b). To determine the number of electrons involved in each process,

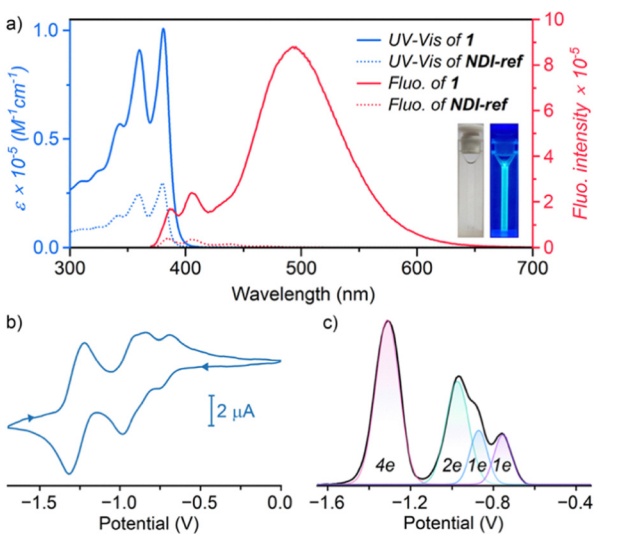


Fig. 2 (a) UV-Vis (6 μM) spectra of **1** and **NDI-ref** and corresponding fluorescence ($\lambda_{ex}$ = 360 nm) spectra in DCM at 298 K. The optical image of the solution of **1** under ambient and UV (365 nm) light. (b) CV of **1** (~0.2 mM) measured using a glassy carbon working electrode and $Ag/AgNO_3$ as reference electrode in DCM with $Bu_4NPF_6$ as supporting electrolyte at 298 K. (c) DPV of **1** (10 mV step pulse). The peaks are deconvoluted to quantify the number of electrons involved in each reduction process. Potentials are given against $Fc/Fc^+$.

differential pulse voltammetry (DPV) was recorded using a 10 mV pulse (Fig. 2c). The deconvolution of reductions spanning −0.6 to −1.1 V reveal two successive one-electron reductions at −0.76 and −0.89 V, followed by a two-electron reduction at −0.97 V. A further intense reduction at −1.31 V was assigned to a four-electron process. Collectively, these electrochemical data indicate that the four NDI units in the oligomer are reduced in a stepwise manner. Each NDI undergoes an initial one-electron reduction over the potential window from −0.5 to −1.1 V, followed by a second reduction at −1.31 V, resulting in an overall eight-electron-reduced state compared to only two and four-electron reduction for **NDI-ref** and **10**, respectively (Fig. S12 and S13). The plausible stepwise reduction process of the NDI units in **1** is given in Fig. S14.

Folding of dye-appended oligomers promotes the formation of stacked chromophore arrays, enabling exciton coupling. In DCM and chloroform, NDI derivatives are efficiently solvated, whereas nonpolar solvents promote aggregation. These effects can be conveniently monitored by UV-Vis spectroscopy following the vibronic intensity ratio ($A_{0-0}/A_{0-1}$) of the $S_0$–$S_1$ transition. It also serves as a useful probe for assessing the extent of intramolecular folding in NDI oligomers.[29] Accordingly, the folding behavior of **1** was examined in two classes of nonpolar solvents, aliphatic and aromatic, which exert distinct effects. In DCM and chloroform (6 μM), **1** exhibits $A_{0-0}/A_{0-1}$ ratios of 1.11 and 1.16, respectively, both significantly lower than that of the reference, **NDI-ref**, which has $A_{0-0}/A_{0-1}$ = 1.20 under identical conditions, indicating a partially folded state (Fig. S15). Addition of cyclohexane (CyHex) to a chloroform solution of **1** led to a relative enhancement of the $A_{0-1}$ band compared to $A_{0-0}$, reducing the $A_{0-0}/A_{0-1}$ ratio to 1.06 at 60% CyHex content (Fig. 3a). This increase in the $A_{0-1}$ contribution reflects enhanced exciton coupling between NDI units as a result of reinforced folding. Similar trends were observed upon addition of other aliphatic hydrocarbons, including *n*-hexane, heptane, octane, and methylcyclohexane (MCH) (Fig. 3c and Fig. S16–S19).

In contrast, aromatic hydrocarbons such as benzene, toluene, *p*-xylene, and mesitylene exert a more pronounced effect, decreasing the $A_{0-0}/A_{0-1}$ ratio to as low as 0.92 in the case of mesitylene (Fig. 3b, d, and Fig. S20–S22). In addition, broad absorption bands appear beyond 400 nm, which is a result of charge-transfer (CT) arising from interactions between the electron-deficient **1** and electron-rich aromatic solvents (Fig. S23).[30] To confirm that these spectral changes originate from intramolecular folding rather than intermolecular aggregation, concentration-dependent UV-Vis measurements were performed over the range of 4–50 μM while maintaining a constant 50% hydrocarbon content (Fig. S24). The invariance of the $A_{0-0}/A_{0-1}$ ratio across this concentration range unambiguously supports an intramolecular folding process.

The effect of aliphatic and aromatic solvents on the emission behaviour of **1** was investigated by recording fluorescence spectra upon incremental addition of these solvents to a chloroform solution of **1** (6 μM). Addition of CyHex (up to 50%) resulted in a pronounced enhancement of the excimer emission (Fig. 4a), accompanied by an increase in the fluorescence quantum yield (QY) from 2.2% in chloroform to 5.1%. Comparable enhancements

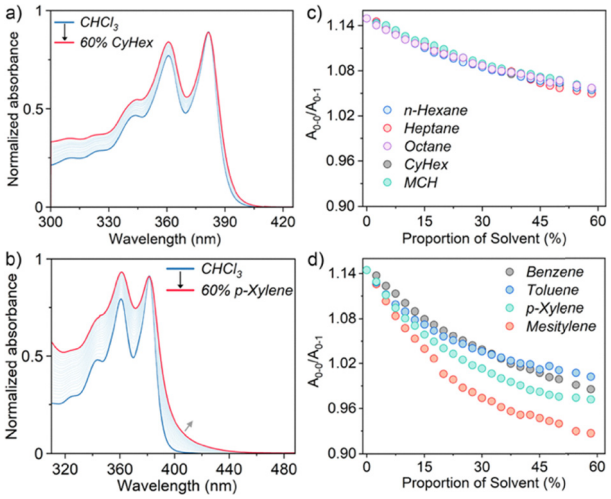


Fig. 3 Relative changes of the $A_{0-1}$ band at 361 nm with respect to the $A_{0-0}$ band at 381 nm in the UV-Vis spectra of **1** (6 μM) in $CHCl_3$ at 298 K upon gradual addition of 60% cyclohexane (a) and *p*-xylene (b). In the case of *p*-xylene, the emergence of a broad absorption band at ∼410 nm is assigned to a charge-transfer (CT) transition arising from interactions between the NDI units and *p*-xylene. Variation of the $A_{0-0}/A_{0-1}$ ratio as a function of increasing proportions of (c) aliphatic and (d) aromatic hydrocarbons, showing a more pronounced effect for aromatic solvents.

were observed for other aliphatic hydrocarbons (Fig. S25), consistent with solvent-induced intramolecular folding that brings the NDI units into proximity, promoting excimer formation. Near constant variation of monomer ($I_{mono}$) and excimer ($I_{ex}$) emission intensity ratio over concentration after addition of 50% of aliphatic solvents further confirms the intramolecular folding responsible for the excimer emission enhancement (Fig. S26). Moreover, the excimer emission of **1** is around six times more intense than that of **10**, and the corresponding QYs are 5.1% and 0.9%, respectively, upon addition of 50% CyHex in chloroform, substantiating the advantage of the tetramer over the dimer analog (Fig. S28).

In contrast, the introduction of aromatic solvents led to more complex photophysical behavior. In all cases, the excimer emission was quenched and accompanied by the emergence of a weak, broad emission band assigned to CT emission (Fig. 4b and Fig. S29). The quenching of the excimer band is attributed to rapid charge transfer from the electron-rich aromatic solvents to the electron-deficient oligomer, resulting in a decrease in fluorescence quantum yield to 0.9% upon addition of 50% toluene. The appearance of CT emission correlates with the emergence of a CT absorption band beyond 400 nm in the UV-Vis studies (Fig. 3b). Moreover, emission maximum systematically red-shifts from ∼495 nm in benzene to ∼540 nm in mesitylene (Fig. 4b), follows the increasing electron-donating strength of the aromatic solvents, further supporting its CT nature. Time-resolved fluorescence decay further corroborates the distinct emission behavior of **1** in aliphatic and aromatic solvents. It shows nearly identical lifetimes of the excimer emission in chloroform before and after addition of aliphatic solvents, confirming that the same emissive state is retained (Fig. 4c and Fig. S31). In contrast, the emissions observed in the presence of aromatic solvents, exhibit faster decay of respective emission maxima and thus shorter lifetimes of 0.8 ns

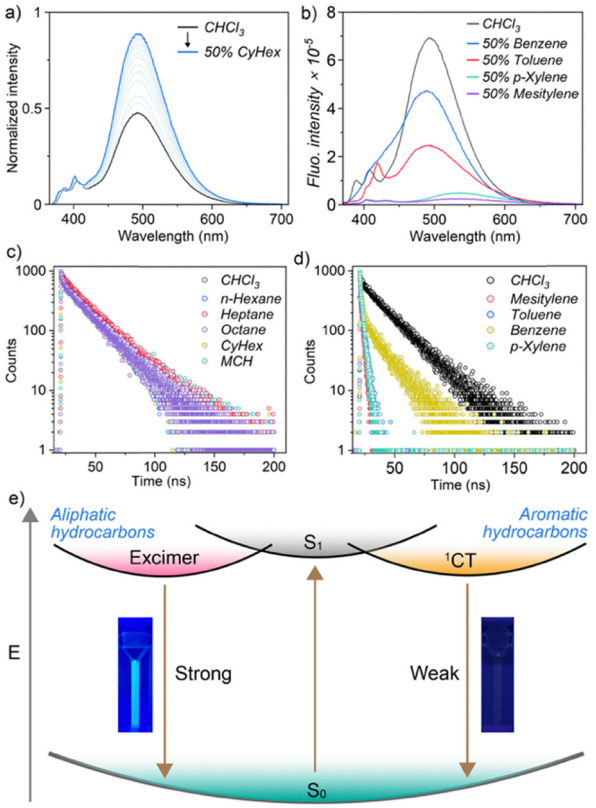


Fig. 4 (a) Change in excimer emission intensity ($\lambda_{ex}$ = 360 nm, normalized at 407 nm) of **1** (6 μM) upon gradual addition of CyHex in $CHCl_3$. (b) Fluorescence spectra of **1** after the addition of 50% aromatic hydrocarbons to the $CHCl_3$ solution, showing quenching of excimer emission and the appearance of CT bands. (c) and (d) Fluorescence decay profiles ($\lambda_{ex}$ = 375 nm) of **1** in $CHCl_3$ and after addition of 50% aliphatic and aromatic hydrocarbons. Monitoring wavelengths are at the respective emission maxima. (e) The schematic illustration shows the overall emission behaviour of **1** in the presence of aliphatic and aromatic hydrocarbons.

for benzene and 0.2 ns for toluene, *p*-xylene, and mesitylene (Fig. 4d and Fig. S32). The significant change in lifetime compared to that of the excimer, along with the solvent-dependent, red-shifted emission, indicates the presence of a CT emissive state.

In summary, we report the synthesis of a flexible, electroactive NDI tetramer, fully characterized by NMR and mass spectrometry. In polar solvents such as DCM and chloroform, it predominantly adopts a partially folded state, as evidenced by the presence of a pronounced excimer emission even at low concentrations ($10^{-7}$ M), a behaviour absent in the **NDI-ref**, a reference monomer. The addition of aliphatic solvents reinforces intramolecular folding, leading to enhanced excimer emission and increased fluorescence quantum yield. In contrast, aromatic solvents disrupt excimer formation through CT interactions, giving rise to weak CT emission resulted in a reduction of overall quantum yield. Notably, this oligomer displays a rare, multifaceted fluorescence response, enabling differentiation between aliphatic and aromatic hydrocarbons. These findings highlight the potential of foldable NDI oligomers as responsive supramolecular systems and applications in molecular sensing and optoelectronic materials.

B. G. conceived the project. D. D. performed the synthesis and conducted the experiments along with D. T. B. G. supervised the research, performed the analysis, and wrote the manuscript. All the authors contributed to the preparation of the final manuscript.

## Conflicts of interest

There are no conflicts to declare.

## Data availability

The data supporting this article have been included as part of the supplementary information (SI). Supplementary information: it contains experimental details, synthetic procedure and characterization data, and additional figures supporting the findings reported in the main text. See DOI: https://doi.org/10.1039/d6cc00572a.

## Acknowledgements

We thank Shiv Nadar Institution of Eminence (SNIoE), Delhi NCR, for financial support and DST-FIST scheme (SR/FST/CS-I/2017/13(C)) for the MALDI facility.

## References

1 S. H. Gellman, *Acc. Chem. Res.*, 1998, **31**, 173–180.
2 D.-W. Zhang, X. Zhao, J.-L. Hou and Z.-T. Li, *Chem. Rev.*, 2012, **112**, 5271–5316.
3 G. Guichard and I. Huc, *Chem. Commun.*, 2011, **47**, 5933–5941.
4 Y. Ferrand and I. Huc, *Acc. Chem. Res.*, 2018, **51**, 970–977.
5 E. A. John, C. J. Massena and O. B. Berryman, *Chem. Rev.*, 2020, **120**, 2759–2782.
6 P. Sang and J. Cai, *Chem. Soc. Rev.*, 2023, **52**, 4843–4877.
7 J. Atcher, P. Mateus, B. Kauffmann, F. Rosu, V. Maurizot and I. Huc, *Angew. Chem., Int. Ed.*, 2021, **60**, 2574–2577.
8 B. Gole, B. Kauffmann, V. Maurizot, I. Huc and Y. Ferrand, *Angew. Chem., Int. Ed.*, 2019, **58**, 8063–8067.
9 L. Sebaoun, V. Maurizot, T. Granier, B. Kauffmann and I. Huc, *J. Am. Chem. Soc.*, 2014, **136**, 2168–2174.
10 C. Yao, B. Gole, A. T. Bui, B. Kauffmann, I. Huc, N. D. McClenaghan and Y. Ferrand, *Chem. Commun.*, 2024, **60**, 8415–8418.
11 S. Samanta and R. K. Roy, *Chem. Sci.*, 2025, **16**, 10325–10332.
12 S. Bhosale, A. L. Sisson, P. Talukdar, A. Fürstenberg, N. Banerji, E. Vauthey, G. Bollot, J. Mareda, C. Röger, F. Würthner, N. Sakai and S. Matile, *Science*, 2006, **313**, 84–86.
13 D. Bialas, A. Zitzler-Kunkel, E. Kirchner, D. Schmidt and F. Würthner, *Nat. Commun.*, 2016, **7**, 12949.
14 Y. Hong, J. Kim, W. Kim, C. Kaufmann, H. Kim, F. Würthner and D. Kim, *J. Am. Chem. Soc.*, 2020, **142**, 7845–7857.
15 E. Kirchner, D. Bialas, F. Fennel, M. Grüne and F. Würthner, *J. Am. Chem. Soc.*, 2019, **141**, 7428–7438.
16 R. Rabban, D. Das, D. Talukdar and B. Gole, *Chem. Commun.*, 2025, **61**, 8071–8074.
17 L. Ernst, H. Song, D. Kim and F. Würthner, *Nat. Chem.*, 2025, **17**, 767–776.
18 A. Schulz, R. Fröhlich, A. Jayachandran, F. Schneider, M. Stolte, T. Brixner and F. Würthner, *Chemistry*, 2024, **10**, 2887–2900.
19 S. K. Keshri, T. Ishizuka, T. Kojima, Y. Matsushita and M. Takeuchi, *J. Am. Chem. Soc.*, 2021, **143**, 3238–3244.
20 A.-B. Bornhof, A. Bauzá, A. Aster, M. Pupier, A. Frontera, E. Vauthey, N. Sakai and S. Matile, *J. Am. Chem. Soc.*, 2018, **140**, 4884–4892.
21 V. Dehm, M. Büchner, J. Seibt, V. Engel and F. Würthner, *Chem. Sci.*, 2011, **2**, 2094–2100.
22 Y. Hong, W. Kim, T. Kim, C. Kaufmann, H. Kim, F. Würthner and D. Kim, *Angew. Chem., Int. Ed.*, 2022, **61**, e202114474.

 

23 X. Hu, J. O. Lindner and F. Würthner, *J. Am. Chem. Soc.*, 2020, **142**, 3321–3325.
24 X. Hu, A. Schulz, J. O. Lindner, M. Grüne, D. Bialas and F. Würthner, *Chem. Sci.*, 2021, **12**, 8342–8352.
25 M. Al Kobaisi, S. V. Bhosale, K. Latham, A. M. Raynor and S. V. Bhosale, *Chem. Rev.*, 2016, **116**, 11685–11796.
26 S. V. Bhosale, M. Al Kobaisi, R. W. Jadhav, P. P. Morajkar, L. A. Jones and S. George, *Chem. Soc. Rev.*, 2021, **50**, 9845–9998.
27 S. Sao, B. R. Samanta and D. Chaudhuri, *RSC Adv.*, 2016, **6**, 34350–34353.
28 M. Kumar and S. J. George, *Nanoscale*, 2011, **3**, 2130–2133.
29 P. Spenst, R. M. Young, B. T. Phelan, M. Keller, J. Dostál, T. Brixner, M. R. Wasielewski and F. Würthner, *J. Am. Chem. Soc.*, 2017, **139**, 2014–2021.
30 C. Kulkarni, G. Periyasamy, S. Balasubramanian and S. J. George, *Phys. Chem. Chem. Phys.*, 2014, **16**, 14661–14664.